Scientia Iranica B (2015) 22(2), 504–518

SCIENTIA IRANICA

Sharif University of Technology
Scientia Iranica
Transactions B: Mechanical Engineering
www.scientiairanica.com

Research Note

Flow and heat transfer characteristics of a viscoelastic fluid over a stretching sheet embedded in a porous medium with meshfree approach

S. Singh* **and R. Bhargava**

Department of Mathematics, Indian Institute of Technology Roorkee, Roorkee, 247667, Uttrakhand, India.

Received 3 November 2012; received in revised form 26 June 2014; accepted 11 August 2014

KEYWORDS
Stretching sheet;
Viscoelastic fluid;
EFGM;
Porous media;
Convective heating.

Abstract. In this article, the flow and heat transfer characteristics in an incompressible, non-Newtonian boundary layer flow of a viscoelastic fluid over a stretching sheet embedded in a porous medium with variable fluid viscosity and thermal conductivity including the effect of viscous dissipation has been examined. The fluid viscosity and thermal conductivity are assumed to be temperature dependent. Unlike the commonly employed thermal conditions of critical and prescribed surface temperature, the present study uses a convective heating boundary condition also along with the prescribed surface temperature condition. The differential equations governing the problem have been transformed by a similarity transformation into a system of non-dimensional differential equations which are solved numerically by Element Free Galerkin Method (EFGM). The effect of various physical parameters like variable fluid viscosity, thermal conductivity, heat source/sink parameter, viscoelastic parameter, porosity parameter, Eckert number, Biot number on velocity, temperature, local skin friction and local heat transfer is studied for both the cases Prescribed Surface Temperature (PST) and Newtonian heating (NH) or convective heating. The present problem finds significant application in chemical engineering, material processing, solar porous wafer absorber systems and metallurgy.

1. Introduction

The flow and heat transfer problems due to a continuously moving stretching surface through an ambient fluid have large applications in many engineering processes, e.g. aerodynamic extrusion of plastic sheets, the cooling of a metallic plate in a cooling bath, the boundary layer along a liquid film in condensation process, and paper production. In these problems, proper understanding of the flow and heat transfer characteristics of the process is quite essential, as fluid used in cooling process and stretching rate have considerable impact upon the quality of the final product.

The behavior of non-Newtonian fluids has been studied through various models in literature. Although, power-law model can describes the behavior of most of the industrial fluids, it does not incorporate another important feature, e.g. the presence of normal stress differences. This normal stress phenomenon is important in lubrication, where the use of liquid between two surfaces help their separation. The simplest subclass of non-Newtonian fluids, known as second grade fluids is capable of describing the normal stress differences, however, it cannot predict the shear thinning and shear thickening properties. The third-

*. *Corresponding author. Tel.: +918527502844; Fax: +91 1332273562*
E-mail addresses: sonaiitr@gmail.com (S. Singh)
rbharfma@iitr.ac.in (R. Bhargava)

grade fluid model is a further attempt towards comprehensive description of these properties. Fluids of grade 'n', informally known as Rivlin and Ericksen [1] fluids, are capable of describing all the properties of non-Newtonian fluids, such as normal stress difference, shear thickening or shear thinning, stress relaxation, creep, elastic effects and memory effects etc.

According to Coleman and Noll [2], the model of an incompressible fluid of grade 'n', includes an indeterminate pressure term and stress terms which are given by a function of velocity gradient and its higher time derivatives:

$$\tau(t) = -pI + \sum_{i=1}^{n} S_i. \tag{1}$$

For $n = 2$, the first two stress tensors S_i are given as:

$$S_1 = \mu A_1, \tag{2}$$

$$S_2 = \alpha_1 A_2 + \alpha_2 (A_1)^2. \tag{3}$$

A_n are the Rivlin-Ericksen tensors defined recursively through:

$$A_1 = (\text{grad}\, V) + (\text{grad}\, V)^{trp}, \tag{4}$$

$$A_2 = \frac{d}{dt} A_1 + A_1.(\text{grad}\, V) + (\text{grad}\, V)^{trp}.A_1, \tag{5}$$

$$A_n = \frac{d}{dt} A_{n-1} + A_{n-1}(\text{grad}\, V) + (\text{grad}\, V)^{trp} A_{n-1},$$
$$n = 2, 3, ... \tag{6}$$

In these equations, V is the velocity, $-pI$ denotes the indeterminate part of the pressure due to the constraint of incompressibility, μ is the viscosity, α_1 and α_2 are the normal stress moduli, β_1, β_2 and β_3 are material moduli which resemble shear dependent viscosity.

In Coleman and Noll model [2], the sign of the material constants α_1 and α_2 is a controversial issue, as discussed by Dunn and Rajagopal [3]. Generally, in the literature, the fluids which satisfies Eq. (3), with $\mu > 0, \alpha_1 \geq 0, \alpha_1 + \alpha_2 = 0$, are known as **second grade fluids**. But, for many of the non-Newtonian fluids of rheological interest, the experimental results for α_1 and α_2 do not satisfy these restrictions. Then, to describe the behavior of such fluids, Fosdick and Rajagopal [4] have found another class of fluids satisfying the relation $\mu > 0, \alpha_1 \leq 0$ and $\alpha_1 + \alpha_2 \neq 0$. These fluids are classified as **second order fluids**. The normal stress effect arises mainly due to elastic nature of the fluid, Walter's liquid B model represents first order approximation for elasticity, i.e. for short or rapidly fading memory fluids. Beard and Walters [5] and Astin et al. [6] developed the boundary layer equations for a modified Oldroyd-B fluid model and the model was solved numerically to study stagnation point flow. The mentioned model is extended to the flow of viscoelastic fluid past a stretching sheet incorporating different physical situations [7]. Rajagopal et al. [8] obtained similarity solutions for flow of a second-order fluid past a stretching sheet with small viscoelastic parameters. Abel et al. [9] studied the non-Newtonian viscoelastic boundary layer flow of Walters' Liquid B past a stretching sheet, taking account of non-uniform heat source and frictional heating.

In all these studies, physical properties of the fluid are considered constants, however, there are some realistic fluids for which viscosity shows a pronounced variation with temperature. Lubricating fluids are such type of fluids in which heat is generated by internal friction and the corresponding rise in the temperature affects the viscosity of the fluid. Hence, the fluid viscosity may no longer remains constant. The effect of variable viscosity and thermal conductivity on MHD viscoelastic fluid flow was analyzed by Prasad et al. [10] and Salem [11]. In these studies, fluid viscosity is considered to vary as an inverse and linear function of temperature.

The study of non-Newtonian fluid flow through porous medium is very important in many industrial applications [12]. In some particular polymer solutions, better volumetric sweep efficiency is achieved in oil displacement mechanism while injected into oil reservoir. Abel and Veena [13] studied the flow and heat transfer characteristics in viscoelastic boundary layer flow in porous medium over a stretching surface. Khani et al. [14] obtained analytical solution for heat transfer of a third grade viscoelastic fluid in non-darcy porous media with thermo-physical effects. However in these studies, the viscous dissipation term in thermal boundary layer equation is taken as $\mu(\partial u/\partial y)^2$, but Al-Hadhrami et al. [15] and Pantokratoras [16] reported that for flow in porous medium, terms of viscous dissipation should be $\mu[u^2/k_p + (\partial u/\partial y)^2]$. Hence, this fact is taken care of in the present study.

In all the above investigations, heat transfer characteristics are examined only for Prescribed Surface Temperature condition (PST), Critical Wall Temperature condition (CWT), Prescribed Heat Flux condition (PHF) and Critical Heat Flux condition (CHF). Heat transfer due to convective boundary conditions was analyzed by Ishak [17], and Makinde and Aziz [18] for simple viscous fluids. Further, Makinde and Aziz [19] extended their work to boundary layer flow of a nanofluid past a stretching sheet with convective boundary condition. In the present study, the behavior of a viscoelastic fluid flow over a stretching sheet embedded in a Darcy porous medium, with variable viscosity and thermal conductivity, has been studied. Heat transfer is considered due to Prescribed Surface

Temperature (PST) and convective boundary conditions or Newtonian Heating (NH).

The mathematical model of the problem has been quite complex due to variable viscosity and modified viscous dissipation terms whose analytical solution is very difficult; therefore numerical technique, EFGM, has been used as a tool to solve the coupled nonlinear partial differential equation governing the flow. Element free Galerkin method has already been successfully employed to solve various problems of heat transfer [20,21].

2. Mathematical model

2.1. Flow analysis

Consider a steady, laminar and two-dimensional flow of an incompressible second order fluid through a porous medium in the presence of viscous dissipation, past an impermeable long continuous stretching sheet. The sheet is coinciding with the plane $y = 0$ and the flow being confined to $y > 0$, as shown in Figure 1. The flow is generated by stretching of an elastic sheet from a slit by two equal and opposite forces in such a way that the origin is fixed and velocity of the sheet is varying linearly with the distance from the slit.

In this two-dimensional model, origin is located at the slit, through which the sheet is drawn through the fluid medium and x and y axes are taken as the coordinates along the sheet and normal to it, respectively. Further u and v are the velocity components along the x and y directions respectively. In x direction, the fluid is moving with velocity u equal to the velocity of the solid surface, whereas at increasing distance from the surface, the fluid velocity is approaching to zero asymptotically. With the usual boundary layer approximation, the governing equations for momentum transfer in Walter's liquid-B model [5,6], in the presence of variable fluid properties (fluid viscosity), take the following from:

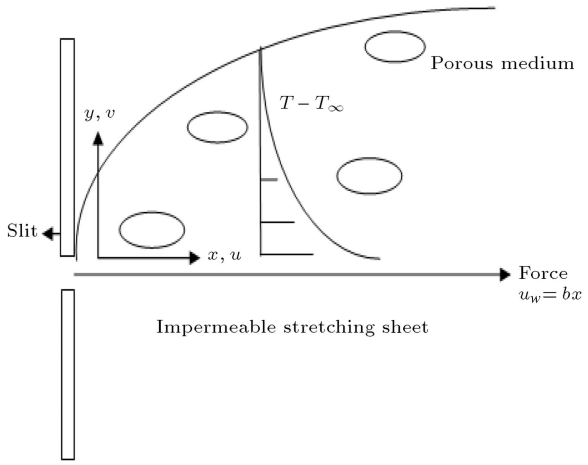

Figure 1. Geometry of the problem.

$$\frac{\partial u}{\partial x} + \frac{\partial v}{\partial y} = 0, \tag{7}$$

$$u\frac{\partial u}{\partial x} + v\frac{\partial u}{\partial y} = \frac{1}{\rho_\infty}\frac{\partial}{\partial y}(\mu\frac{\partial u}{\partial y}) - k_0(u\frac{\partial^3 u}{\partial x \partial y^2} + v\frac{\partial^3 u}{\partial y^3} + \frac{\partial u}{\partial x}\frac{\partial^2 u}{\partial y^2} - \frac{\partial u}{\partial y}\frac{\partial^2 u}{\partial x \partial y}) - \frac{\mu u}{\rho_\infty k_p}. \tag{8}$$

The last two terms on the right hand side of the momentum equation designate the Darcian bulk impedance. All the fluid properties are assumed to be isotropic and constant, except for the thermal conductivity and fluid viscosity. Fluid viscosity, μ, is assumed to vary as an inverse and linear function of temperature, T, as proposed in [10,11]:

$$\frac{1}{\mu} = \frac{1}{\mu_\infty}[1 + \gamma(T - T_\infty)]. \tag{9}$$

Eq. (9) can be rewritten as:

$$\frac{1}{\mu} = a(T - T_r),$$

where:

$$a = \frac{\gamma}{\mu_\infty} \quad \text{and,} \quad T_r = T_\infty - \frac{1}{\gamma}. \tag{10}$$

Here a and T_r both are constants and their values depend upon the reference sate and the thermal property of the fluid, i.e. κ. T_∞ and μ_∞ are temperature and coefficient of viscosity, respectively far away from the sheet. In general $a > 0$ (i.e. $\gamma > 0$) corresponds to liquid and $a < 0$ (i.e. $\gamma < 0$) for gases. Another constant, θ_r, is defined as [22]:

$$\theta_r = \frac{T_r - T_\infty}{T_w - T_\infty} = -\frac{1}{\gamma(T_w - T_\infty)}. \tag{11}$$

From the above analysis of γ, it can be easily observed that θ_r is negative for liquids and positive for gases. Also from Eq. (11), $\theta_r \to \infty$ implies either γ or temperature difference $(T_w - T_\infty)$ is negligibly small, and for $(\gamma \to 0)$, from Eq. (9), $\mu = \mu_\infty =$ constant, i.e. the effect of variable viscosity can be neglected and a constant value of viscosity can be assumed throughout the boundary layer.

Now substituting Eq. (9) into Eq. (8), we obtain the system of equations as:

$$\frac{\partial u}{\partial x} + \frac{\partial v}{\partial y} = 0, \tag{12}$$

$$u\frac{\partial u}{\partial x}+v\frac{\partial u}{\partial y}=\frac{1}{\rho_\infty}\frac{\partial}{\partial y}\left(\frac{\mu_\infty}{1+\gamma(T-T_\infty)}\frac{\partial u}{\partial y}\right)$$
$$-k_0\left(u\frac{\partial^3 u}{\partial x\partial y^2}+v\frac{\partial^3 u}{\partial y^3}+\frac{\partial u}{\partial x}\frac{\partial^2 u}{\partial y^2}-\frac{\partial u}{\partial y}\frac{\partial^2}{\partial x\partial y}\right)$$
$$-\frac{1}{\rho_\infty}\left(\frac{\mu_\infty}{1+\kappa(T-T_{infty})}\frac{u}{k_p}\right). \quad (13)$$

2.2. Boundary conditions

The boundary conditions on the velocity field are given as:

$$u=u_w=bx, v=0 \qquad \text{at} \quad y=0 \quad (14)$$

$$u\to 0, u_y\to 0 \qquad \text{at} \quad y\to\infty. \quad (15)$$

In Eq. (15), an augmented boundary condition for longitudinal velocity gradient, which implies absence of shear stress in free stream, has been added up following Fosdick and Rajagopal [4]. The momentum equation given in Eq. (13) is a third order differential equation in u and without this augmented boundary condition the prescribed boundary conditions on u are two. Therefore, adherence boundary conditions are insufficient to determine unique solution of the above system, and imposition of this boundary condition becomes necessary.

Such kind of mismatching of boundary conditions is reported in literature in most of the boundary flow problems of viscoelastic fluids over moving surfaces. It leads to the non-uniqueness of the solution as suggested by Chang [23]. To overcome this insufficiency of boundary condition, Rajagopal [8], Mahapatra and Gupta [7] assumed the solution as series expansion of the dependent quantity up to the first order of viscoelastic parameter. They omitted higher order terms of k_0^2 and k_0^3, as in the case of boundary layer flow of viscoelastic fluid with short memory; the characteristic time scale associated with the motion is large as compared to the relaxation time of the fluid. This expansion of solution would reduce the order of differential equation by one and makes the order of the governing equation equal to the number of prescribed boundary conditions. To facilitate a computational solution and to provide results that hold good for any scale of parameter, we choose the boundary conditions as given in Eqs. (14) and (15).

2.3. Transformation of the model

For non-dimensionalization of system of equations (12)-(14), the following transformations are used:

$$u=bxf_\eta(\eta), \quad v=-(b\nu_\infty)^{-1/2}f(\eta),$$
$$\eta=\sqrt{\frac{b}{\nu_\infty}}y, \quad \theta(\eta)=\frac{T-T_\infty}{T_w-T_\infty}. \quad (16)$$

By employing these transformations, Eq. (12) is automatically satisfied and Eq. (13) reduces to:

$$f_\eta^2-ff_{\eta\eta}=\frac{1}{1-\theta/\theta_r}\left(f_{\eta\eta\eta}-\frac{f_{\eta\eta}\theta_\eta}{\theta-\theta_r}\right)$$
$$-k_1(2f_\eta f_{\eta\eta\eta}-ff_{\eta\eta\eta}-f_{\eta\eta}^2)$$
$$-\left(\frac{\theta_r}{\theta_r-\theta}\right)K^*f_\eta, \quad (17)$$

and the corresponding boundary conditions are transformed to:

$$f(\eta)=0, \quad f_\eta(\eta)=1 \qquad \text{at} \quad \eta=0, \quad (18)$$

$$f_\eta(\eta)=0, \quad f_{\eta\eta}(\eta)=0 \qquad \text{at} \quad \eta\to\infty, \quad (19)$$

where $k_1=\frac{k_0 b}{\nu_\infty}$ is the dimensionless viscoelastic parameter, $\theta_r=-\frac{1}{\gamma(T_w-T_\infty)}$ is the fluid viscosity parameter, and its value is determined by the viscosity of the fluid and the operating temperature difference. $K^*=\frac{\nu_\infty}{bk_p}$ is the porosity parameter. For $\theta_r\to\infty$, or in case of constant viscosity, the analytical solution of Eq. (17) with boundary conditions (Eq. (18)) can be given as:

$$f(\eta)=\frac{1-e^{-\zeta\eta}}{\zeta} \quad \text{where} \quad \zeta=\sqrt{\frac{1+K^*}{1-k_1}}. \quad (20)$$

Using Eq. (20) into Eq. (16), the velocity components are obtained:

$$u=bxe^{-\zeta\eta} \quad \text{and} \quad v=-(b\nu_\infty)^{1/2}\left(\frac{1-e^{-\zeta\eta}}{\zeta}\right). \quad (21)$$

From Eq. (20), for viscoelastic flow, viscoelastic parameter, k_1, should lie between 0 and 1, i.e. $0<k_1<1$, while $k_1=0$ implies a purely viscous fluid. For a purely viscous fluid and with constant thermophysical property ($\theta_r\to\infty$), Eq. (17) reduces to $f_{\eta\eta\eta}+ff_{\eta\eta}-f_\eta^2-K^*f_\eta=0$ which is satisfied by Eq. (30) with $k_1=0$ (i.e. $\zeta=\sqrt{1+K^*}$). It is in agreement with the steady sate flow's solution for a purely viscous fluid.

The non-dimensional local shear stress on the surface of the stretching sheet is given by:

$$c_f=\frac{\tau_w}{\rho_\infty u_w^2}=\mathrm{Re}_x^{-1/2}\left(\frac{\theta_r}{\theta_r-\theta}\right)f_{\eta\eta}(0),$$

where:

$$\tau_w=\mu\left(\frac{\partial u}{\partial y}\right)|_{y=0} \quad (22)$$

$$\Rightarrow c_f\mathrm{Re}_x^{1/2}=\left(\frac{\theta_r}{\theta_r-\theta}\right)f_{\eta\eta}(\eta) \quad \text{at} \quad \eta=0, \quad (23)$$

where $Re_x=\frac{bx^2}{\nu}$ is the local Reynolds Number.

3. Heat transfer analysis

The governing boundary layer heat transfer equation, including variable thermal conductivity and viscous dissipation effect, is written as:

$$\rho_\infty c_p(u\frac{\partial T}{\partial x}+v\frac{\partial T}{\partial y})=\mu(\frac{u^2}{k_p}+(\frac{\partial u}{\partial y})^2) + \frac{\partial}{\partial y}(K(T)\frac{\partial T}{\partial y})+Q_s(T-T_\infty). \quad (24)$$

Thermal conductivity of the fluid is also assumed to be temperature dependent and is given in the following form, as suggested by Prasad et al. [10]:

$$K(T)=k_\infty(1+\frac{\epsilon}{\Delta T}(T-T_\infty)), \quad (25)$$

where $\Delta T=T_w-T_\infty$, T_w is the sheet temperature, k_∞ is the thermal conductivity of the fluid far away from the sheet, and ϵ is a small parameter. Now by substituting Eq. (25) into Eq. (24), it reduces to:

$$\rho_\infty c_p u\frac{\partial T}{\partial x}+(\rho_\infty c_p v-\frac{k_\infty\epsilon}{\Delta T}\frac{\partial T}{\partial y})\frac{\partial T}{\partial y} = (\frac{\mu}{1+\gamma(T-T_\infty)}(\frac{u^2}{k_p}+(\frac{\partial u}{\partial y})^2) + (k_\infty(1+\frac{\epsilon}{\Delta T}(T-T_\infty)))\frac{\partial^2 T}{\partial y^2} + Q_s(T-T_\infty). \quad (26)$$

3.1. Boundary conditions

In this study, for heat transfer analysis, two types of boundary conditions, namely, Prescribed Surface Temperature (PST) and Newtonian Heating or Convective Heating (NH) conditions, are considered.

Prescribed Surface Temperature (PST case). The boundary conditions for this case are given as:

$$T=T_W=T_\infty+B(\frac{x}{l})^2 \quad \text{at} \quad y=0, \quad (27)$$

$$T=T_\infty \quad \text{as} \quad y\to\infty, \quad (28)$$

where B is a constant, and l is the characteristic length. Boundary condition in Eq. (27) is considered for mathematical simplification and to vanish x from the both sides of Eq. (24) which finally converts coupled partial differential equations to coupled ordinary differential equations. Defining the non-dimensional temperature $\theta(\eta)$ as:

$$\theta(\eta)=\frac{T-T_\infty}{T_w-T\infty}, \quad (29)$$

and substituting Eqs. (16), (27) and (28) into Eq. (26), it can be rewritten as:

$$(1+\epsilon\theta)\theta_{\eta\eta}+\epsilon\theta_\eta^2+\Pr(f\theta_\eta-(2f_\eta-\beta)\theta + \mathrm{Ec}\frac{1}{(1-\theta/\theta_r)}(K^*f_\eta^2+f_{\eta\eta}^2))=0, \quad (30)$$

where $\Pr=\frac{\mu_\infty c_p}{k_\infty}$ is the Prandtl number, and $\Pr^*=\Pr(1-\frac{\theta}{\theta_r})^{-1}$ is the modified Prandtl number due to variable viscosity inside the boundary layer region, $\beta=\frac{Q_s}{\rho_\infty c_p b}$ is the heat source/sink parameter, $\mathrm{Ec}=\frac{b^2l^2}{Ac_p}$ is the Eckert Number. Consequently, the boundary conditions (Eqs. (27) and (28)) take the form:

$$\theta(\eta)=1 \quad \text{at} \quad \eta=0 \quad \text{and} \quad \theta(\eta)=0 \quad \text{at} \quad \eta\to\infty. \quad (31)$$

Newtonian heating or convective heating conditions (NH case). In this heating process, the left surface of the sheet is heated by convection from a hot fluid at temperature T_f with heat transfer coefficient h_f. In this case, the sheet surface temperature, T_w, is not known a priori like PST case, but it is to be determined later as the result of a convective heating process from the hot fluid at temperature T_f. Under this assumption, using Newtonian's law of cooling, the boundary conditions for the thermal field may be written as [17,18]:

$$-k\frac{\partial T}{\partial y}=h_f(T_f-T_w) \quad \text{at} \quad y=0 \quad \text{and} \quad T\to T_\infty \quad \text{as} \quad y\to\infty. \quad (32)$$

The non-dimensional temperature, $\theta(\eta)$, is given as:

$$\theta(\eta)=\frac{T-T_\infty}{T_f-T_\infty} \quad \text{where} \quad T_f-T_\infty=D(\frac{x}{l})^2. \quad (33)$$

Now using the transformations given in Eqs. (16) and (33) into Eq. (30) and boundary conditions given in Eq. (31), the heat transport equation remains the same and the corresponding boundary conditions are transformed to:

$$\theta_\eta(\eta)=-\mathrm{Bi}(1-\theta(\eta)) \quad \text{at} \quad \eta=0 \quad \text{and} \quad \theta(\eta)=0 \quad \text{as} \quad \eta\to\infty, \quad (34)$$

where $\mathrm{Bi}=\frac{h_f}{k}\sqrt{\frac{\nu_\infty}{b}}$ is the Biot number. For $\mathrm{Bi}\to\infty$, this boundary condition reduces to $\theta(0)=1$.

The local heat transfer rate in terms of Nusselt number can be expressed as:

$$\mathrm{Nu}_x=\frac{xq_w}{K(T_w-T_\infty)}=-\mathrm{Re}_x^{1/2}\theta_\eta(0),$$

where:

$$q_w = -K(\frac{\partial T}{\partial y})|_{y=0}, \tag{35}$$

i.e.:

$$\mathrm{Nu}_x \mathrm{Re}_x^{-1/2} = -\theta_\eta(\eta) \quad \text{at} \quad \eta = 0. \tag{36}$$

4. Numerical solution

For the solution of system of simultaneous differential equation given in Eqs. (16) and (30), with Conditions (18), (19), (31) and (34), the equations are reformulated as:

$$f_\eta - h = 0, \tag{37}$$

$$h^2 - fh_\eta - \frac{1}{(1-\theta/\theta_r)}(h_{\eta\eta} - \frac{h_\eta \theta_\eta}{\theta - \theta_r}) + k_1(2hh_{\eta\eta} - fh_{\eta\eta\eta} - h_\eta^2) + (\frac{\theta_r}{\theta_r - \theta})K^* h = 0, \tag{38}$$

$$(1+\epsilon\theta)\theta_{\eta\eta} + \epsilon\theta_\eta^2 + \mathrm{Pr}(f\theta_\eta - (2h-\beta)\theta + \frac{\mathrm{Ec}}{(1-\theta/\theta_r)}(K^* h^2 + h_\eta^2)) = 0. \tag{39}$$

And the corresponding boundary conditions now become:

$$f(\eta) = 0, \quad h(\eta) = 1, \quad \text{at} \quad \eta = 0, \tag{40}$$

$$h(\eta) = 0, \quad h_\eta(\eta) = 0, \quad \theta(\eta) = 0 \quad \text{as} \quad \eta \to \infty, \tag{41}$$

along with the two cases:

$$\theta(\eta) = 1 \quad (\mathrm{PST}) \quad \text{and}$$

$$\theta_\eta(\eta) = -\mathrm{Bi}(1-\theta(\eta)) \quad (\mathrm{NH}) \quad \text{at} \quad \eta = 0. \tag{42}$$

The numerical solution of the system of simultaneous differential equations given in Eqs. (37)-(39) along with the boundary conditions (Eqs. (40)-(42)) is obtained using Element Free Galerkin Method (EFGM).

4.1. Element free Galerkin method

The Element Free Galerkin Method (EFGM) requires Moving Least Square (MLS) interpolation functions to approximate an unknown function. Using MLS approximation, the unknown field variable $u(x)$ is approximated over the two-dimensional domain Ω as (details can be seen in [24]):

$$u^h(x) = \sum_{I=1}^{n^*} \Phi_I(x) u_I = \mathbf{\Phi}(\mathbf{x})\mathbf{u}. \tag{43}$$

The shape function $\Phi_I(x)$ is defined by:

$$\Phi_I(x) = \sum_{j=1}^{m} p_j(x)(A^{-1}(x)B_j(x))_{jI} = p^T A^{-1} B_I,$$

$$A(x) = \sum_{I=1}^{n^*} W(x - x_I)p(x_I)p^T(x_I),$$

$$B(x) = [W(x-x_1)p(x_1), W(x-x_2)p(x_2), ..., W(x-x_{n^*})p(x_{n^*}), \tag{44}$$

where $p(x)$ is a vector of complete basis function of order m. In present study, we have used a linear basis function in two dimensions, i.e. $p^T(x) = [1 \;\; x \;\; x^2]$. $W(x - x_I)$ is a weight function, which is non-zero over a small neighborhood of a particular quadrature point or evaluation point, that small neighborhood area is called support domain of the quadrature point, n^* is the number of nodes that are included in the support domain of an evaluation point x.

4.2. Weight function description

The choice of weight function affects the resulting approximation in EFGM and other meshless methods. In EFGM, the continuity of MLS approximants is governed by the continuity of weight function. Singh et al. [25] have studied these weight functions and reported that cubicspline weight function gives more accurate results as compared to others. Therefore, in present work, cubic spline weight function has been used.

Cubic spline weight function

$$W(\mathbf{x} - \mathbf{x}_I) = w(\bar{r}) = \begin{pmatrix} \frac{2}{3} - 4\bar{r}^2 + 4\bar{r}^3 & \bar{r} \le \frac{1}{2} \\ \frac{4}{3} - 4\bar{r} + 4\bar{r}^2 - \frac{4}{3}\bar{r}^3 & \frac{1}{2} < \bar{r} \le 1 \\ 0 & \bar{r} > 1 \end{pmatrix}, \tag{45}$$

where $\bar{r} = \frac{\|\mathbf{x}-\mathbf{x}_I\|}{d_{mI}}$, $\|\mathbf{x} - \mathbf{x}_I\|$ is the distance from an evaluation point $\mathbf{x}$ to node $\mathbf{x}_I$, d_{mI} is related to the size of support domain and it is calculated as $d_{mI} = D_{\max} C_I$, where $d_{\max}$ is a scaling parameter and C_I is the distance to nearest neighbor from evaluation point. The size of the support domain d_{mI} is mostly controlled by the scaling parameter as the distance between nearest neighbors for an evaluation point remains unchanged for a given uniform nodal data distribution. To preserve the non-singularity of weighted moment matrix $\mathbf{A}$, it is required that minimum value of $d_{\max} > 1$, so that $n > m$ and maximum value of $d_{\max}$ must be chosen in such a way that local character of MLS approximation is ensured. In the present simulation, value of $d_{\max}$ has been fixed as 2.2.

4.3. Weighted integral formulation for EFGM

The weighted integral form of Eqs. (37)-(39) over the entire domain can be written as:

$$\int_0^{\eta_{\max}} w_1(f_\eta - h)d\eta = 0, \tag{46}$$

$$\int_0^{\eta_{\max}} w_2(h^2 - fh_\eta - \frac{1}{(1-\theta/\theta_r)}\left(h_{\eta\eta} - \frac{h_\eta\theta_\eta}{\theta-\theta_r}\right) + k_1(2hh_{\eta\eta} - fh_{\eta\eta\eta} - h_\eta^2) + \left(\frac{\theta_r}{\theta_r-\theta}\right)K^*h)d\eta = 0, \tag{47}$$

$$\int_0^{\eta_{\max}} w_3((1+\epsilon\theta)\theta_{\eta\eta} + \epsilon\theta_\eta^2 + \Pr(f\theta_\eta - (2h-\beta)\theta + \frac{Ec}{(1-\theta/\theta_r)}(K^*h^2 + h_\eta^2)))d\eta = 0, \tag{48}$$

where w_1, w_2 and w_3 are arbitrary test functions and may be viewed as the variation in f, h and θ, respectively, and $\eta_{\max}$ denotes the length of boundary layer region.

4.4. Element free Galerkin model and construction of MLS shape functions

The Element free Galerkin model of Eqs. (46)-(48) may be obtained by substituting MLS approximation for the unknown variables f, h and θ using Eqs. (43) and (44).

$$f = \sum_{I=1}^{n^*}\Phi_I f_I, \quad h = \sum_{I=1}^{n^*}\Phi_I h_I, \quad \theta = \sum_{I=1}^{n^*}\Phi_I\theta_I. \tag{49}$$

For construction of MLS shape functions, quadratic basis functions $p^T(X) = [1 \;\; x \;\; x^2]$ with cubic spline weight functions and rectangular support domains are used. We opted for quadratic basis functions due to presence of higher order derivative terms in momentum equations. A uniform size of the support domain, for all the quadrature points has been considered and the value of scaling parameter $d_{\max}$ is taken as 2.2. In Table 1, shape functions for some of the quadrature points (marked as stars in Figure 2) are shown. For all the quadrature points, in whole domain, the computation of shape functions is done in similar manner.

4.5. Imposition of boundary conditions using penalty method

Using penalty method to enforce the essential boundary conditions, the integral form of the equations is written as:

$$\int_0^{\eta_{\max}} w_1(f_\eta - h)d\eta + \bar{\alpha}w_1(f - f(0))|_{\eta=0} = 0, \tag{50}$$

$$\int_0^{\eta_{\max}} w_2(h^2 - fh_\eta - \frac{1}{(1-\theta/\theta_r)}\left(h_{\eta\eta} - \frac{h_\eta\theta_\eta}{\theta-\theta_r}\right)$$

Table 1. Construction of MLS shape functions.

Quadrature point	Number of nodes in the support domain	Nodes in the support domain	Shape functions
(1.2035,0)	5	(1.1500,0)	$338.0 - 556.0x + 228.5x^2$
		(1.1750,0)	$-147.6 + 251.4x - 106.8x^2$
		(1.2000,0)	$-360.3 + 601.5x - 250.7x^2$
		(1.2250,0)	$-138.7 + 226.6x - 92.28x^2$
		(1.2500,0)	$309.6 - 523.5x + 221.3x^2$
(1.2465,0)	5	(1.2000,0)	$381.2 - 602.6x + 238.1x^2$
		(1.2250,0)	$-187.6 + 305.8x - 124.4x^2$
		(1.2500,0)	$-398.3 + 638.4x - 255.5x^2$
		(1.2750,0)	$-113.4 + 176.4x - 68.37x^2$
		(1.3000,0)	$319.1 - 517.9x + 210.1x^2$
(1.2165,0)	4	(1.1750,0)	$600.7 - 979.1x + 398.9x^2$
		(1.2000,0)	$-577.0 + 957.2x - 396.6x^2$
		(1.2250,0)	$-598.0 + 982.8x - 403.4x^2$
		(1.2500,0)	$575.3 - 960.9x + 401.1x^2$
(1.2335,0)	4	(1.2000,0)	$636.8 - 1018x + 406.4x^2$
		(1.2250,0)	$-635.5 + 1033x - 419.2x^2$
		(1.2500,0)	$-588.5 + 947.2x - 380.8x^2$
		(1.2750,0)	$588.2 - 962.4x + 393.6x^2$

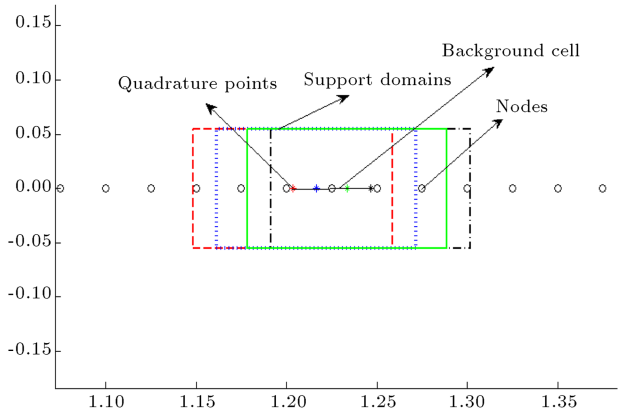

Figure 2. Schematic view of nodal discretization and support domains of various quadrature points.

$$+k_1(2hh_{\eta\eta}-fh_{\eta\eta\eta}-h_\eta^2)+\left(\frac{\theta_r}{\theta_r-\theta}\right)K^*h)d\eta$$
$$+\bar{\alpha}w_2(h-h(0))|_{\eta=0}$$
$$+\bar{\alpha}w_2(h-h(\eta_{\max}))|_{\eta=\eta_{\max}}=0, \quad (51)$$

$$\int_0^{\eta_{\max}} w_3((1+\epsilon\theta)\theta_{\eta\eta}+\epsilon\theta_\eta^2+\Pr(f\theta_\eta-(2h-\beta)\theta$$
$$+\frac{\mathrm{Ec}}{(1-\theta/\theta_r)}(K^*h^2+h_\eta^2)))d\eta$$
$$+\bar{\alpha}w_3(\theta-\theta(0))|_{\eta=0}$$
$$+\bar{\alpha}w_3(\theta-\theta(\eta_{\max}))|_{\eta=\eta_{\max}}=0, \quad (52)$$

where $f(0)=0$, $h(0)=1$, $h(\eta_{\max})=0$, $\theta(0)=1$ (for PST case), $\theta(0)=(\theta_\eta(0)+\mathrm{Bi})/\mathrm{Bi}$ (for NH case), $\theta(\eta_{\max})=0$ as given in Eqs. (40)-(42). w_1, w_2 and w_3 are to be replaced by the MLS shape functions $\Phi_I(I=1,2,...,N)$ (N denotes the total number of nodes in the whole computational domain). The penalty parameter $\bar{\alpha}$, in present work, is chosen as 10^6. Using the EFGM model given by Eq. (49) into Eqs. (50)-(52), the system of equations can be defined by matrix form, which is given as follows:

$$\begin{bmatrix} K_{11} & K_{12} & K_{13} \\ K_{21} & K_{22} & K_{23} \\ K_{31} & K_{32} & K_{33} \end{bmatrix} \begin{bmatrix} f \\ h \\ \theta \end{bmatrix} = \begin{bmatrix} H_1 \\ H_2 \\ H_3 \end{bmatrix}, \quad (53)$$

where $[K_{mn}]$ and $[H_m](m,n=1,2,3)$ are as follows:

$$(K_{11})_{IJ}=\int_0^{\eta_{\max}}\Phi_I\frac{d\Phi_J}{d\eta}d\eta+\bar{\alpha}\Phi_I\Phi_J|_{\eta=0},$$
$$(K_{12})_{IJ}=\int_0^{\eta_{\max}}-\Phi_I\Phi_J d\eta,$$
$$(K_{13})_{IJ}=0, \qquad (K_{21})_{IJ}=0,$$
$$(K_{22})_{IJ}=\int_0^{\eta_{\max}}(\Phi_I\Phi_J\bar{h}-\Phi_I\frac{d\Phi_J}{d\eta}\bar{f}$$
$$+\left(\frac{\theta_r}{\theta_r-\bar{\theta}}\right)\frac{d\Phi_I}{d\eta}\frac{d\Phi_J}{d\eta}-2k_1\frac{d\Phi_I}{d\eta}\frac{d\Phi_J}{d\eta}\bar{h}$$
$$-k_1\frac{d^2\Phi_I}{d\eta^2}\frac{d\Phi_J}{d\eta}\bar{f}-k_1\Phi_I\frac{d\Phi_J}{d\eta}\frac{d\bar{h}}{d\eta}$$
$$+\left(\frac{\theta_r}{\theta_r-\bar{\theta}}\right)K^*\Phi_I\phi_J)d\eta+\bar{\alpha}\Phi_I\Phi_J|_{\eta=0}$$
$$+\bar{\alpha}\Phi_I\Phi_J|_{\eta=\eta_{\max}},$$
$$(K_{23})_{IJ}=\int_0^{\eta_{\max}}-\frac{\theta_r}{(\theta-\theta_r)^2}\Phi_I\frac{d\Phi_J}{d\eta}\frac{d\bar{h}}{d\eta}d\eta,$$
$$(K_{31})_{IJ}=\int_0^{\eta_{\max}}\Pr\Phi_I\Phi_J\frac{d\bar{\theta}}{d\eta}d\eta,$$
$$(K_{32})_{IJ}=\int_0^{\eta_{\max}}(-2\Pr\Phi_I\Phi_J\bar{\theta}$$
$$+\Pr.\mathrm{Ec}\left(\frac{\theta_r}{\theta_r-\bar{\theta}}\right)(K^*\Phi_I\Phi_J\bar{h}$$
$$+\Phi_I\frac{d\Phi_J}{d\eta}\frac{d\bar{h}}{d\eta}))d\eta,$$
$$(K_{33})_{IJ}=\int_0^{\eta_{\max}}\left(-\frac{d\Phi_I}{d\eta}\frac{d\Phi_J}{d\eta}-\epsilon\frac{d\Phi_I}{d\eta}\frac{d\Phi_J}{d\eta}\bar{\theta}\right.$$
$$\left.+\epsilon\Phi_I\frac{d\Phi_J}{d\eta}\frac{d\bar{\theta}}{d\eta}+\Pr\beta\Phi_I\Phi_J\right)d\eta$$
$$+\bar{\alpha}\Phi_I\Phi_J|_{\eta=0}+\bar{\alpha}\Phi_I\Phi_J|_{\eta=\eta_{\max}},$$
$$(H_1)_I=\bar{\alpha}f(0)\Phi_I|_{\eta=0},$$
$$(H_2)_I=\bar{\alpha}h(0)\Phi_I|_{\eta=0}+\bar{\alpha}h(\eta_{\max})\Phi_I|_{\eta=\eta_{\max}},$$
$$(H_3)_I=\bar{\alpha}\theta(0)\Phi_I|_{\eta=0}+\bar{\alpha}\theta(\eta_{\max})\Phi_I|_{\eta=\eta_{\max}},$$

with:

$$(I,J)=(1,2,...,N),$$

with:

$$\bar{f}=\sum_{I=1}^{n^*}\Phi_I\bar{f}_I, \quad \bar{h}=\sum_{I=1}^{n^*}\Phi_I\bar{h}_I, \quad \bar{\theta}=\sum_{I=1}^{n^*}\Phi_I\bar{\theta}_I. \quad (54)$$

The computational domain Ω is discretized with uniformly distributed 201 nodes. The length of the boundary layer region, i.e. $\eta_{\max}$, is chosen as 5.0. Results were obtained even for large values of $\eta_{\max}$, but beyond 5.0 length; no appreciable effect on results

was observed. Therefore, for demonstration purpose, we restricted the boundary layer thickness as 5.0. Four-point Gauss quadrature formula has been used to calculate the integral values. At each node, three functions f, h and θ are to be evaluated, hence, after assembly, we obtain a non-linear system of equations of order 603×603, as given in Eq. (53).

Owing to the nonlinearity of the system, an iterative scheme has been used to solve it with an initial guess. The system of equations is linearized by incorporating known functions $\bar{f}, \bar{h}$ and $\bar{\theta}$, which are calculated using the known values of variables f, h and θ at node I on previous iteration, as given in Eq. (54), and then whole system is solved using Gauss elimination method. This gives a new set of values of unknowns f, h and θ and the process continues till the required accuracy of 5×10^{-4} is achieved.

4.6. Validation of the results

For validation purpose, results are compared with some results reported by Chen [26] and Grubka and Bobba [27], in Table 2, and a good agreement can be observed between them; a grid convergence study is also done to check their consistency.

5. Numerical results and discussions

Figures 3 and 4 depict the effect of viscoelastic parameter, k_1, on velocity profile, $f_\eta(\eta)$, and non-dimensional velocity stream function, $f(\eta)$. From Figures 3 and 4, it is observed that velocity decreases with the increase of viscoelastic parameter, k_1. This result is consistent with the fact that the introduction of tensile stress due to the viscoelasticity causes transverse contraction of the boundary layer and hence velocity decrease.

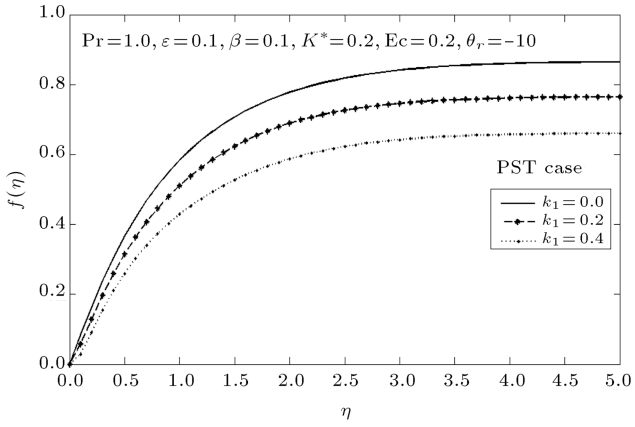

Figure 3. Velocity stream function, $f(\eta)$, for different values of viscoelastic parameter, k_1.

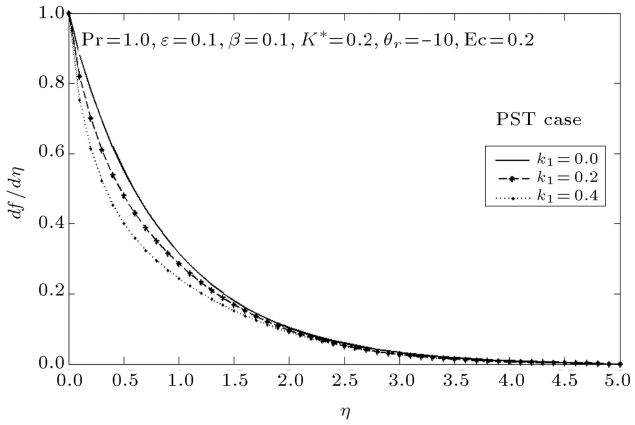

Figure 4. Velocity distribution $f_\eta(\eta) = df/d\eta$ for different values of viscoelastic parameter, k_1.

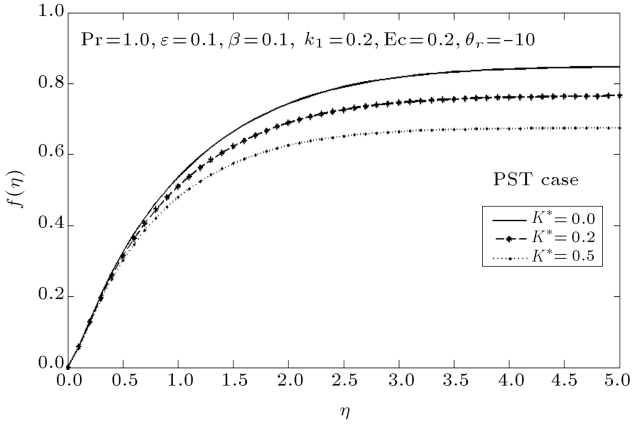

Figure 5. Velocity stream function, $f(\eta)$, for different values of porosity parameter, K^*.

In Figures 5 and 6, the effect of porosity parameter, K^*, on velocity profile, $f_\eta(\eta)$, and non-dimensional velocity stream function, $f(\eta)$, is observed. An increment in the porosity parameter, K^*, corresponds to a decrease in permeability parameter, k_p, i.e. decrease in porosity (pore size decreases). Thus, obstruction in the

Table 2. Comparison of results for the Nusselt number, $-\theta_\eta(0)$, with Chen [26], Grubka and Bobba [27] results for, $k_1 = 0$, $K^* = 0$, $1/\theta_r = 0$, $\epsilon = 0$, $\beta = 0$, Ec $= 0$ and various values of Pr.

Pr	Chen [26]	Grubka and Bobba [27]	Present results with 101 nodes	Present results with 201 nodes	Present results with 501 nodes
1.0	1.33334	1.3333	1.3333	1.3333	1.3333
2.0	-	-	1.9874	1.9876	1.9876
3.0	2.50972	2.5097	2.5090	2.5095	2.5095
5.0	-	-	3.6572	3.6577	3.6577
10.0	4.79686	4.7969	4.7965	4.7968	4.7968

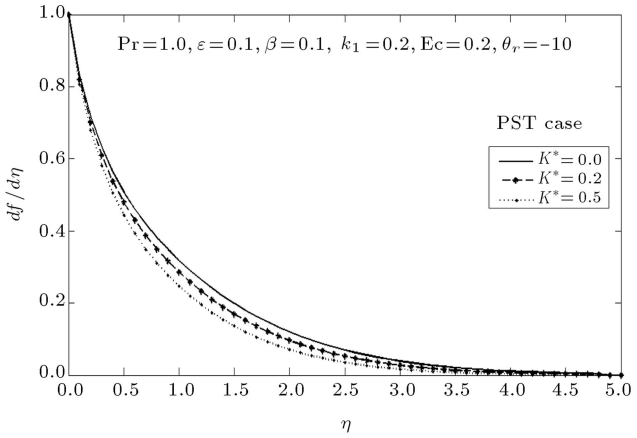

Figure 6. Velocity distribution, $f_\eta(\eta) = df/d\eta$, for different values of porosity parameter, K^*.

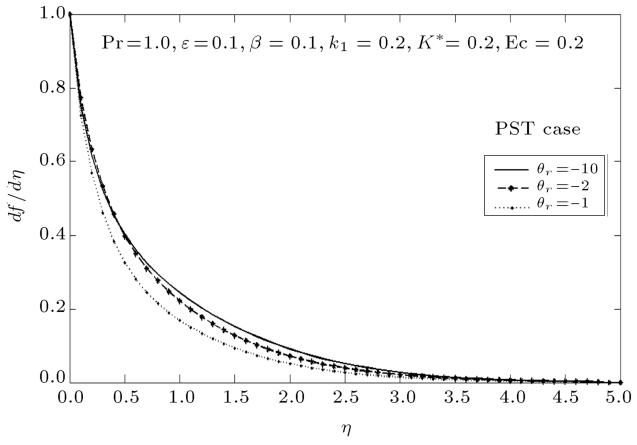

Figure 7. Velocity distribution $f_\eta(\eta) = df/d\eta$ for different values of eter, θ_r.

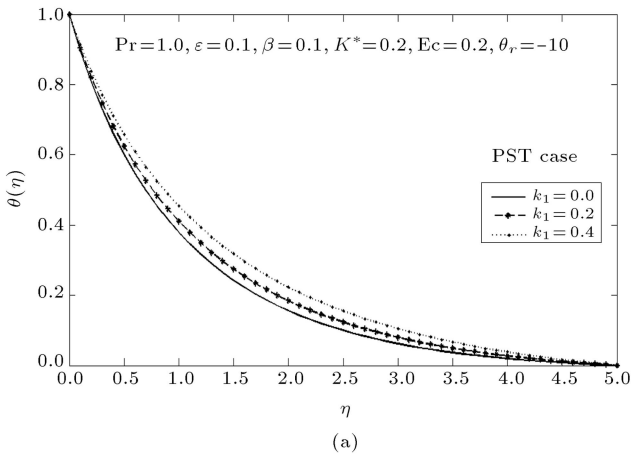

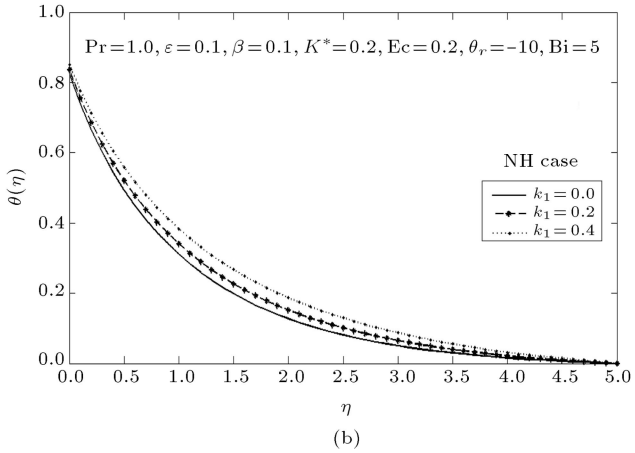

Figure 8. Temperature distribution, $\theta(\eta)$, for different values of viscoelastic parameter, k_1, for (a) PST, and (b) NH cases.

motion of the fluid increases as the pore size decreases. Therefore, velocity decreases in the boundary layer with increase in porosity parameter, K^*. The presence of porous medium with low permeability can be used as a mechanism for depressing velocities, i.e. decelerating flow in industrial applications. Similar effect of parameter K^* is observed on the non-dimensional velocity stream function, $f(\eta)$.

Figure 7 shows the effect of fluid viscosity parameter, θ_r, on velocity profile, $f_\eta(\eta)$. It shows that velocity decreases with increase in θ_r, as expected, since highly viscous fluids have lesser velocity.

Figure 8(a) and (b) depict the temperature profile, $\theta(\eta)$, for different values of viscoelastic parameter, k_1, for PST case and NH cases, respectively. It is observed that temperature increases with the rise of viscoelasticity for both the PST and NH cases. This is due to the fact that an increase of viscoelastic normal stress gives rise to thickening of thermal boundary layer. Similar effect of porosity parameter, K^*, on temperature profile, $\theta(\eta)$, is observed for both the cases PST and NH in Figure 9(a) and (b).

Figure 10(a) and (b) reveal the effect of Prandtl Number Pr on heat transfer process in PST and NH cases, respectively. It is seen that the effect of increasing Prandtl number, Pr is to decrease temperature throughout the boundary layer, which results in decrease of the thermal boundary layer thickness. The increase of Prandtl number implies slow rate of thermal diffusion.

Figure 11(a) and (b) illustrate that the effect of increasing values of Eckert number, Ec, is to increase temperature distribution in the flow region in both the PST and NH cases. This behavior of temperature enhancement occurs as heat energy is stored in the fluid due to frictional heating.

Figure 12(a) and (b) are drawn for temperature profile, $\theta(\eta)$, for various values of the thermal conductivity parameter, ϵ, for both PST and NH cases. Both the graphs demonstrate that an increase in the value of thermal conductivity parameter, ϵ, results in increase of temperature.

The temperature profile, $\theta(\eta)$, for different values of heat source/sink parameter, β, is shown in Figure 13(a) and (b) for both the PST and NH cases.

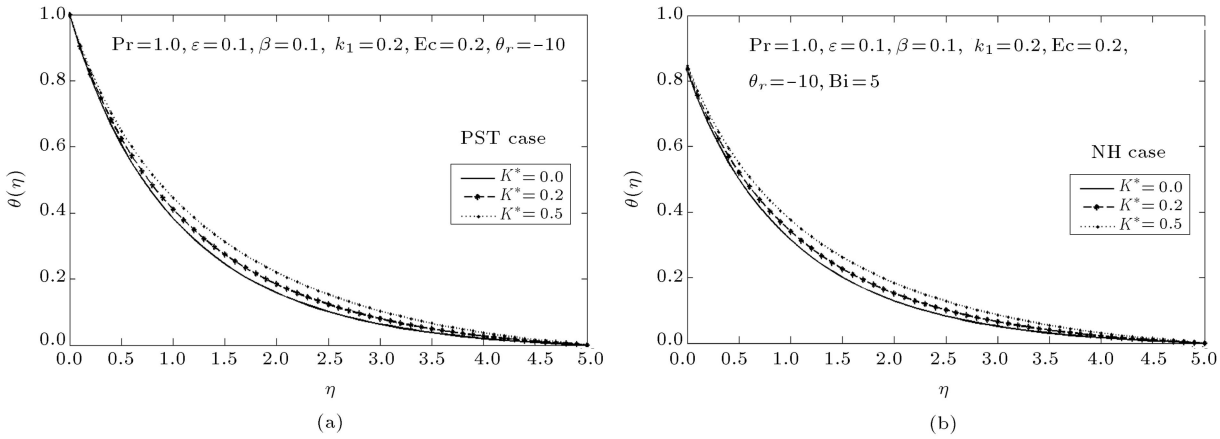

Figure 9. Temperature distribution, $\theta(\eta)$, for different values of porosity parameter, K^*, for (a) PST, and (b) NH cases.

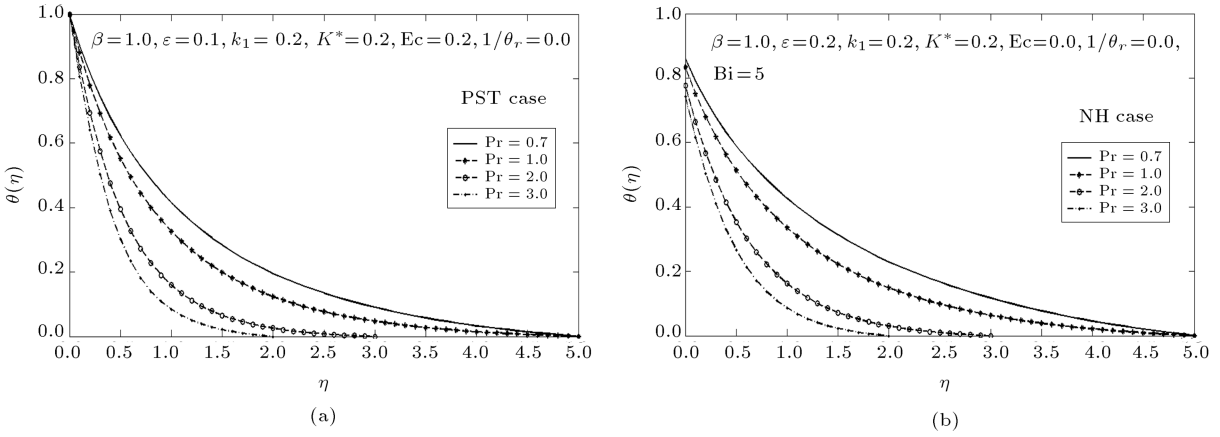

Figure 10. Temperature distribution, $\theta(\eta)$, for different values of Prandtl number, Pr, for (a) PST, and (b) NH cases.

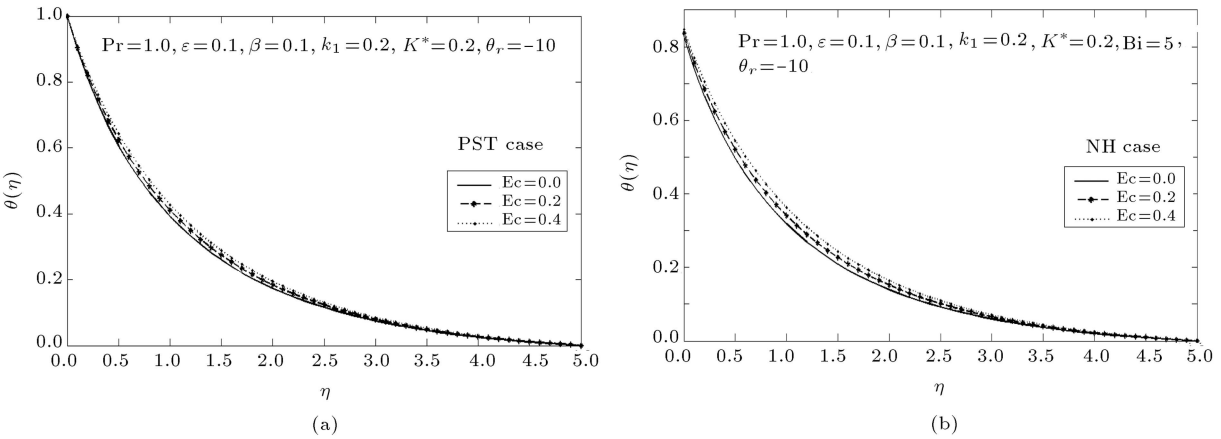

Figure 11. Temperature distribution, $\theta(\eta)$, for different values of Eckert number, Ec, for (a) PST, and (b) NH cases.

It is observed that the temperature profile is lower throughout the boundary layer for negative values of β (heat sink), and higher for positive values of β (heat source) as compared with the temperature profile in the absence of heat source/sink parameter, i.e. $\beta = 0$. Physically, $\beta > 0$ implies $T_w > T_\infty$, i.e. there will be a supply of heat to the fluid from the wall. Similarly, $\beta < 0$ implies $T_w < T_\infty$ and there will be a transfer of heat from the fluid to the wall. The effect of increasing the value of heat source/sink parameter, β, is to increase the temperature profile.

The graphs for temperature profile, $\theta(\eta)$, for various values of the fluid viscosity parameter, θ_r, for PST and NH cases are shown in Figure 14(a) and (b). These figures indicate that increases in the values of

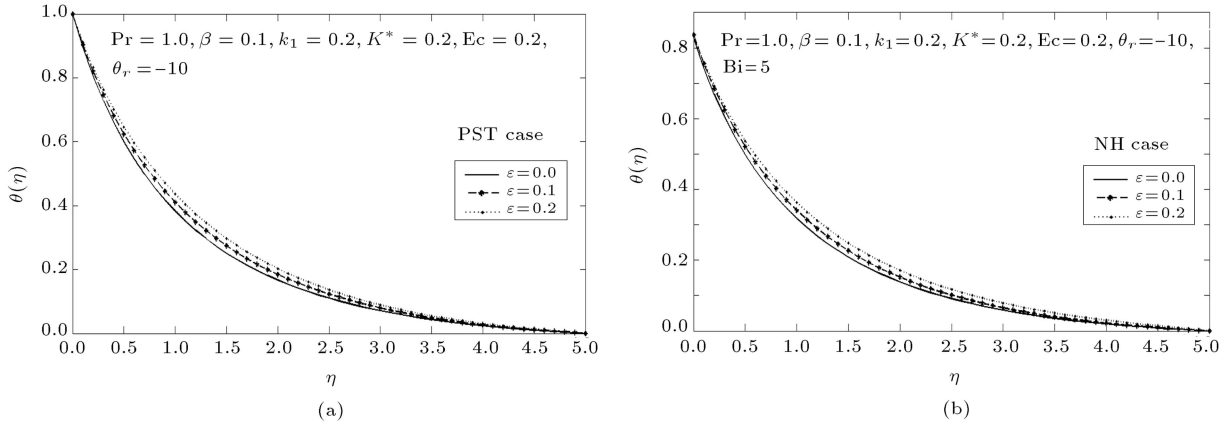

Figure 12. Temperature distribution, $\theta(\eta)$, for different values of thermal conductivity parameter, ϵ, for (a) PST, and (b) NH cases.

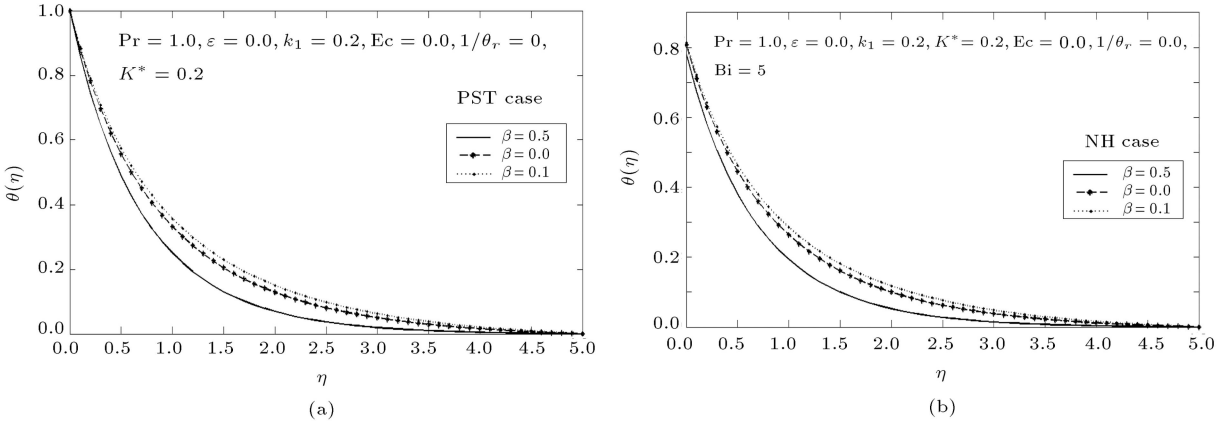

Figure 13. Temperature distribution, $\theta(\eta)$, for different values of heat source/sink parameter, β, for (a) PST, and (b) NH cases.

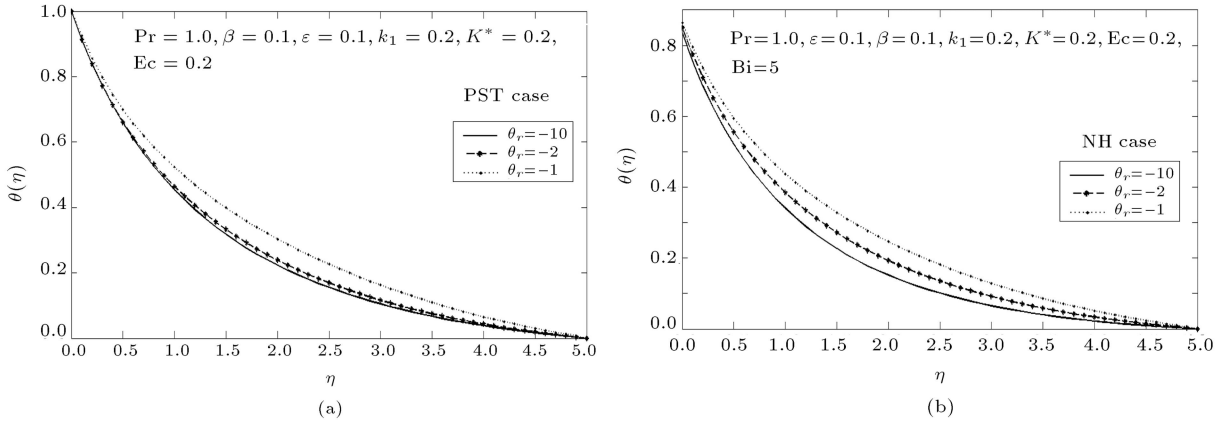

Figure 14. Temperature distribution, $\theta(\eta)$, for different values of viscosity parameter, θ_r, for (a) PST, and (b) NH cases.

θ_r have the tendency to increase the thermal boundary layer thickness for both the cases.

In PST case, the wall temperature is unity for all the parameters. However, for the NH case, it is different for different parameters due to adiabatic boundary conditions. The results of NH case are qualitatively similar to that of PST case but quantitatively they are different.

Figure 15 illustrates the effect of Biot number Bi on temperature profile, $\theta(\eta)$, for NH case. Biot number (Bi) is the ratio of the internal thermal resistance of a solid to the boundary layer thermal resistance. When Bi $\rightarrow$ 0 (i.e. for very small values of Biot number), the left side of the plate with hot fluid is insulated, the internal thermal resistance of the plate is extremely high, and no convective heat transfer

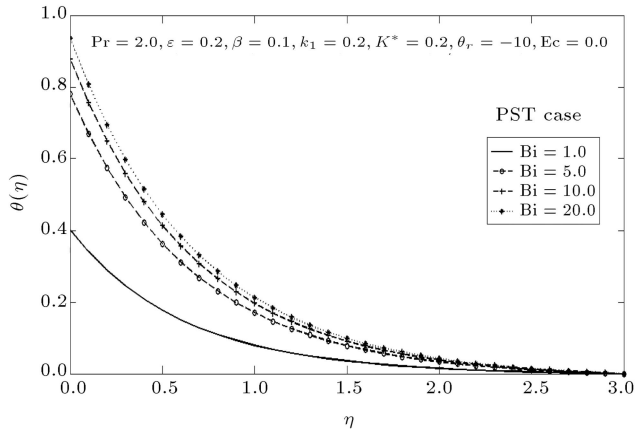

Figure 15. Temperature distribution, $\theta(\eta)$, for different values of Biot number, Bi, for NH case.

Table 3. Heat transfer rate $\mathrm{Nu}_x\mathrm{Re}_x^{-1/2}$ for different parameters.

Parameters	Values	$-\boldsymbol{\theta_\eta(0)}$ (PST)	$-\boldsymbol{\theta_\eta(0)}$ (NH)
k_1	0.0	1.0550	0.8737
	0.2	0.9691	0.8140
	0.4	0.8670	0.7430
Pr	0.7	0.9910	0.6974
	1.0	1.1922	0.8310
	2.0	1.6500	1.1190
	3.0	1.9374	1.2840
K^*	0.0	1.0190	0.8515
	0.2	0.9695	0.8140
	0.5	0.9030	0.7660
Ec	0.0	1.0281	0.8650
	0.2	0.9690	0.8143
	0.4	0.9090	0.7640
θ_r	-10.0	0.9695	0.8140
	-2.0	0.8653	0.7500
	-1.0	0.7582	0.6790
Bi	1		0.5991
	5		1.1024
	10		1.2230
	20		1.2920

from the hot fluid at the left of the plate to the cold fluid on the right side of the plate takes place. Figure 15 shows that temperature increases with the rise of Biot number. The result is consistent with the fact that stronger convection results in higher surface temperatures, causing the thermal effect to penetrate deeper into the quiescent fluid.

Tables 3 and 4 reveal the effect of various physical parameters on local skin friction and heat transfer rate, respectively, for both the cases PST and NH.

Table 4. Skin friction coefficient for different values of viscoelastic parameter, k_1, porosity parameter, K^*, and viscosity parameter, θ_r, keeping Pr=1.0, $\epsilon = 0.1$, $\beta = 0.1$, Ec=0.2 and Bi=5.0.

Parameters	Values	$\boldsymbol{f_{\eta\eta}(0)}$(PST)	$\boldsymbol{f_{\eta\eta}(0)}$(NH)
k_1	0.0	-1.2021	-1.1913
	0.2	-1.8012	-1.7804
	0.4	-2.4830	-2.4560
K^*	0.0	-1.6981	-1.6761
	0.2	-1.8013	-1.7800
	0.5	-1.9311	-1.9110
θ_r	-10.0	-1.8014	-1.7803
	-2.0	-2.273	-2.1921
	-1.0	-2.7492	-2.6302

6. Conclusions

The main findings can be summarized as:

1. The effect of viscoelastic, fluid viscosity and porosity parameter is to decrease the velocity distribution.
2. The effect of increasing values of viscoelastic parameter, fluid viscosity, porosity parameter, Eckert number is to increase the temperature significantly in the boundary layer flow. The temperature, thus, can be varied to desired value with increment in viscoelastic effect.
3. The thermal boundary layer thickness decreases with the increase of Prandtl Number.
4. The effect of thermal conductivity is to increase the temperature distribution; hence fluids with less thermal conductivity may be opted for effective cooling.
5. The temperature profile is lower throughout the boundary layer for heat-sink parameter, and higher for heat-source parameter.
6. Temperature increases with an increase in the convective heat transfer parameter, i.e. the Biot number (Bi).

Nomenclature

x	Flow directional coordinate along the stretching sheet
y	Along normal to the stretching sheet
u, v	Velocity components along x, y direction
T	Temperature
B, D	Prescribed constants
l	Characteristic length
c_p	Specific heat
k_0	Coefficient of viscoelasticity

k_1	Dimensionless viscoelastic parameter
$K*$	Porosity parameter
Pr	Prandtl number
b	Linear stretching rate
k_p	Permeability of the porous medium
Bi	Biot number
Ec	Eckert number
c_f	Skin friction
τ_w	Wall shearing stress
Nu_x	Local Nusselt number
Re_x	Local Reynolds number

Greek symbols

θ	Dimensionless temperature
η	Dimensionless space variable
μ	Coefficient of viscosity
ν	Coefficient of dynamic viscosity
ρ	Density

Subscripts

w, ∞	Conditions along the sheet and free stream, respectively

References

1. Rivlin, R.S. and Ericksen, J.L. "Stress deformation relations for isotropic materials", *Journal of Rational Mechanics and Analysis*, **4**, p. 323 (1955).
2. Coleman, B.D. and Noll, W. "An approximate theorem for functionals with applications in continuum mechanics", *Archive for Rational Mechanics and Analysis*, **56**, p. 191 (1965).
3. Dunn, J.E. and Rajagopal, K.R. "Fluids of differential type - critical review and thermodynamic analysis", *International Journal of Engineering Science*, **33**, pp. 689-729 (1995)
4. Fosdick, R.L. and Rajagopal, K.R. "Thermodynamics and stability analysis of fluids of third grade", *Proceedings of the Royal Society of London*, **369**, pp. 351-377 (1980).
5. Beard, D.W. and Walter, K. "Elastico-viscous boundary layer flows 1, two dimensional flow near a stagnation point", *Proceedings of Cambridge Philosophical Society*, **60**, pp. 667-674 (1964).
6. Astin, J., Jones, R.S. and Lockyer, P. "Boundary layers in non-Newtonian fluids", *Journal of Mechanics*, **12**, pp. 527-539 (1973).
7. Mahapatra, T.R. and Gupta, A.S. "Stagnation-point flow of a visco-elastic fluid towards a stretching surface", *International Journal of Non-linear Mechanics*, **39**, pp. 811-820 (2004).
8. Rajagopal, K.R., Na, T.Y. and Gupta, A.S. "Flow of viscoelastic fluid due to stretching sheet", *Rheological Acta*, **23**, pp. 213-215 (1984).
9. Abel, M.S., Siddheshwar, P.G. and Nandeppanavar, M.M. "Heat transfer in a viscoelastic boundary layer flow over a stretching sheet with viscous dissipation and non-uniform heat source", *International Journal of Heat and Mass Transfer*, **50**, pp. 960-966 (2007).
10. Prasad, K.V., Pal, D., Umesh, V. and Rao, P.N.S. "The effect of variable viscosity on MHD viscoelastic fluid flow and heat transfer over a stretching sheet", *Communications in Non-linear Science and Numerical Simulation*, **15**, pp. 331-344 (2010).
11. Salem, A.M. "Variable viscosity and thermal conductivity effects on MHD flow and heat transfer in viscoelastic fluid over a stretching sheet", *Physics Letters A*, **369**, pp. 315-322 (2007).
12. Roy, S., Junk, M. and Sundar, S. "Understanding the porosity dependence of heat flux through glass fiber insulation", *Mathematical and Computer Modelling*, **43**, pp. 485-492 (2006).
13. Abel, M.S. and Veena, P. "Viscoelastic fluid flow and heat transfer in a porous medium over a stretching sheet", *International Journal of Non-linear Mechanics*, **33**(3), pp. 531-540 (1998).
14. Khani, F., Farmany, A., Raji, M.A., Aziz, A. and Samadi, F. "Analytic solution for heat transfer of a third grade viscoelastic fluid in non-darcy porous media with thermophysical effects", *Communications in Non-linear Science and Numerical Simulation*, **14**, pp. 3867-3878 (2009).
15. Al-Hadhrami, A.K., Elliott, L. and Ingham, D.B. "A new model for viscous dissipation in a porous medium across a range of permeability values", *Transportation in Porous Media*, **53**, pp. 117-122 (2003).
16. Pantokratoras, A. "Comment on "numerical study for micropolor flow over a stretching sheet" by Moncef Aouadi (computational materials science, 38 (2007), 774-780)", *Computational Materials Science*, **42**, pp. 717-718 (2008).
17. Ishak, A. "Similarity solutions for flow and heat transfer over a permeable surface with convective boundary condition", *Applied Mathematics and Computation*, **217**, pp. 837-842 (2010).
18. Makinde, O.D. and Aziz, A. "MHD mixed convection from a vertical plate embedded in a porous medium with a convective boundary condition", *International Journal of Thermal Science*, **49**, pp. 1813-1820 (2010).
19. Makinde, O.D. and Aziz, A. "Boundary layer flow of a nano fluid past a stretching sheet with a convective boundary condition", *International Journal of Thermal Science*, **50**, pp. 1326-1332 (2011).
20. Bhargava, R. and Singh, S. "Numerical simulation of unsteady MHD flow and heat transfer of a second grade fluid with viscous dissipation and joule heating using meshfree approach", *World Academy of Science, Engineering and Technology*, **66**, pp. 1215-1221 (2012).
21. Singh, S. and Bhargava, R. "Numerical study of natural convection within a wavy enclosure using meshfree approach: Effect of corner heating", *The Scientific*

World Journal, 2014, Article ID 842401, 18 pages, dx.doi.org/10.1155/2014/842401 (2014).

22. Pal, D. and Mondal, H. "Effect of variable viscosity on MHD non-darcy mixed convective heat transfer over a stretching sheet embedded in a porous medium with non-uniform heat source/sink", *Communications in Non-linear Science and Numerical Simulation*, **15**, pp. 1553-1564 (2010).
23. Chung, W.D. "The non-uniqueness of the flow of viscoelastic fluid over a stretching sheets", *Quarterly of Applied Mathematics*, **47**, pp. 365-366 (1989).
24. Liu, G.R., *Meshfree Methods-Moving Beyond the Finite Element Method*, CRC press, London (2003).
25. Singh, A., Singh, I.V. and Prakash, R. "Numerical analysis of fluid squeezed between two parallel plates by meshless method", *Computer & Fluids*, **36**, pp. 1460-1480 (2007).
26. Chen, C.H. "Laminar mixed convection adjacent to vertical, continuously stretching sheets", *Heat and Mass Transfer*, **33**, pp. 471-476 (1998).
27. Grubka, L.T. and Bobba, K.M. "Heat transfer characteristic of a continuous stretching surface with variable temperature", *ASME Journal of Heat Transfer*, **107**, pp. 248-250 (1985b).

Biographies

Sonam Singh has completed her Ph.D. degree from department of mathematics, I.I.T. Roorkee, India, under the supervision of Prof. Rama Bhargava. Currently, she is working as an assistant professor at University of Delhi. Her area of interest is computational fluid dynamics, numerical techniques, finite element and meshfree methods.

Rama Bhargava is a professor at Department of Mathematics, I.I.T. Roorkee, India. Her fields of specialization include computational fluid dynamics, computer graphics, bio-mathematic, finite element and meshfree methods. She has research and teaching experience of around 35 years at I.I.T. Roorkee. She has completed many projects and has more than hundred publications in international journals in her fields of expertise.